ChemComm

Cite this: *Chem. Commun.*, 2012, **48**, 422–424

www.rsc.org/chemcomm

COMMUNICATION

Superparamagnetic Fe_3O_4 nanoparticles–carbon nitride nanotube hybrids for highly efficient peroxidase mimetic catalysts†

Jung Woo Lee,[a] Hyung Joon Jeon,[a] Hyun-Joon Shin[b] and Jeung Ku Kang*[a]

Received 16th September 2011, Accepted 28th October 2011
DOI: 10.1039/c1cc15725f

We report a facile route to synthesize size tunable Fe_3O_4 nanoparticles (NPs)–carbon nitride nanotube (CNNT) hybrids. These hybrids showing the water-soluble property are proven to exhibit ultra high peroxidase mimetic activity compared to those of pure NPs, where a colorless peroxidase substrate 3,3,5,5-tetramethylbenzidine changes by H_2O_2 to its blue colored oxidized state.

Zero dimensional (0D) nanoparticles (NPs) such as quantum dots have been intriguing in many state-of-the-art applications.[1–3] Similarly, the one dimensional (1D) nanostructures such as carbon nanotubes (CNTs) with conspicuous aspect ratios have been shown to exhibit remarkable properties.[4–6] Meanwhile, the hybrid nanostructures fabricated in conjunction with NPs and CNTs have been proven to be capable of showing much more advanced synergic performances.[7–12] Also, processes such as coal conversion as well as manufacture of polymer materials such as dyes, resins, and plastics discharge wastewater containing harmful organics that are suggested to be capable of causing cancers.[13] In this view, enzymes such as horseradish peroxidase effective in decomposing organic compounds by catalyzing oxidation in the presence of H_2O_2 to form oligomers have recently attracted great attention.[14]

However, the problem is in that these peroxidase enzymes lost their original catalytic activity under certain pH and temperature conditions. Also, they could be decomposed through digestion by proteases. Meanwhile, it has been recently demonstrated that pure Fe_3O_4 NPs could show the peroxidase mimetic activity for the reactions including the oxidation of organic substrates such as 3,3,5,5-tetramethylbenzidine (hereafter, we call it TMB) to reduce their toxicity, whose product color change has been generally used in wastewater treatment detection,[15,16] as described in Fig. 1. However, pure NPs still involve the intricacy of the synthesis procedure with agglomeration[17–19] resulting in a significant deterioration of their original activity. Herein, we report a facile method to synthesize highly efficient peroxidase mimetic superparamagnetic Fe_3O_4 NPs–carbon nitride nanotube (CNNT) hybrid catalysts using an instant microwave heating assisted liquid polyol process. The attached NPs on CNNTs were found to be of uniform size without showing the agglomeration observed on pure nanoparticle catalysts. Also, our N K-edge near edge X-ray absorption fine structure (NEXAFS) analysis demonstrates that the NPs-hybrid structure has been fabricated *via* the so-called direct "N-mediated nucleation" using N atoms of CNNTs.

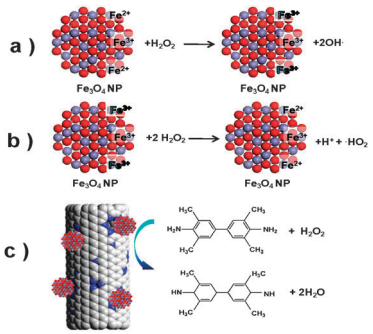

Fig. 1 Schematics of (a) oxidation and (b) reduction processes on Fe_3O_4 NPs in the presence of H_2O_2, and (c) the peroxidase mimetic reaction of the TMB substrate by the Fe_3O_4 NPs–CNNT hybrid catalyst. (C: white sphere, N: blue sphere, Fe: light purple sphere, O: red sphere).

First, CNNTs were synthesized by microwave plasma enhanced chemical vapor deposition using Fe catalysts prepared using radio frequency magnetron sputtering on the SiO_x/Si substrate. Next, the magnetite NP precursors were dispersed onto the grown CNNTs in a liquid polyol solution. Finally, the instant microwave heating for a few minutes was applied to the solution for anchoring magnetite NPs on the surface layers of CNNTs. Fig. 2a and b show the scanning electron microscopy (SEM) and the transmission electron microscopy (TEM) images of pristine CNNTs, respectively, where the average length and the external diameter of vertically aligned CNNTs are of about 48 μm and 15 nm in size with turbostratic graphene structures. We find that the sizes of well-dispersed magnetite NPs on the CNNTs are tunable on different concentrations of $Fe(acac)_3$ and reaction times. Fig. 2c, d and f show TEM images of size controlled magnetite NPs on the surface monolayers of CNNTs. The initial nucleation of NPs (see Fig. 2c) was observed to occur using 200 mg of $Fe(acac)_3$ and 90 s of microwave heating (denoted H-1). The NPs with angular shape are of an average size of 2.3 nm. Also, the high angle

[a] *Graduate School of EEWS, Department of Materials Science & Engineering, NanoCentury KAIST Institute, KAIST, 291 Daehak-ro, Yuseong Gu, Daejeon, Republic of Korea. E-mail: jeungku@kaist.ac.kr; Fax: +82-42-350-3310; Tel: +82-42-350-3338*
[b] *Pohang Accelerator Laboratory, Department of Physics, Pohang University of Science and Technology, San 31, Hyojadong, Pohang 790-784, Republic of Korea*
† Electronic supplementary information (ESI) available. See DOI: 10.1039/c1cc15725f

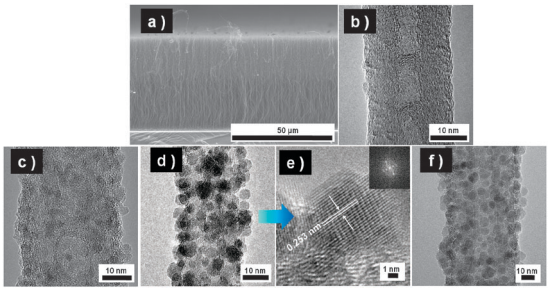

Fig. 2 (a) SEM image of as-synthesized CNNTs. (b) TEM image of a pristine CNNT. TEM images representing (c) 2.3 nm (H-1), (d) 4.9 nm (H-2), and (f) 7.9 nm (H-4) sizes of NPs attached on CNNTs, respectively. (e) HRTEM image of a NP of the H-2 sample. Inset: FFT of the NP.

annular dark field (HADDF) image and the line scan of energy dispersive X-ray spectroscopy (EDS) of H-1 (Fig. S1a, ESI†) demonstrate that NPs reside with very uniform sizes on the surface layers of CNNTs. In addition, the EDS analysis (Fig. S1b, ESI†) shows that concentrations of Fe and O elements are 2.37 and 3.11 atomic %, respectively. As the reaction time increases to 120 s and 150 s (denoted H-2 and H-3), their average sizes are found to increase to 4.9 nm and 7.9 nm, respectively, as seen in Fig. 2d and f. In addition, the lattice spacing of 0.253 nm and its fast Fourier transformation image with the (311) plane (Fig. 2e) for H-2 demonstrate that the magnetite NP is in a crystalline phase. Meanwhile, when we use double the amount of the iron oxide precursor (400 mg) while maintaining the same reaction time as that used to synthesize H-2 (Fig. S1c, ESI†), the density of NPs on the CNNT is found to become higher, although their average size decreases to 4.0 nm from 4.9 nm.

Fig. 3a shows the X-ray diffraction (XRD) patterns for CNNTs, Fe_3O_4 NPs, and Fe_3O_4 NPs–CNNT hybrid structures. First of all, pure CNNTs had three peaks at 25.99, 42.94, and 53.62°, matching with the (002), (101), and (004) planes of graphite (JCPDS, 41-1487), respectively. These peaks are attributed to the ~3.4 Å interlayer distance between graphene layers of the nanotube. Pure Fe_3O_4 NPs used as a reference (Fig. S4, ESI†) show peaks at 18.28, 30.17, 35.5, 37.13, 43.15, 53.57, 57.2, and 62.8°, corresponding to the (111), (220), (311), (222), (400), (422), (522), and (440) planes of the magnetite structure (JCPDS, 19-0629), respectively. Additionally, the sample treated for 90 s (H-1) was found to show a large broad peak related to the nucleation stage of NPs. Also, the relatively decreased XRD intensity is considered to be attributed to the dense coverage of Fe_3O_4 NPs on the CNNT surface. Meanwhile, the 150 s-heated samples show higher peak sharpness of the (311) plane than that for the 120 s-heated ones, implying that the NP size is increased. In addition, we performed the NEXAFS analysis for both CNNTs and NP–CNNT hybrids to investigate the binding mechanism between NPs and CNNTs (see Fig. 3b). The CNNTs give three different graphite-like nitrogen (GN), the pyridine-like nitrogen (PN), and N_2 states. This demonstrates that molecular nitrogen exists in the hollow compartment of CNNTs. Because of a long probing depth,[20] we could analyze the more refined nitrogen states for NP–CNNT hybrids *via* the NEXAFS measurements. The N K-edge NEXAFS spectra consist of three peaks, around 397, 401, and 407 eV (denoted I, II, and III, respectively), where I represents the electron transition from 1 s to the unoccupied π* state of GN and PN in the CNNTs. The π* feature of N_2 gas in CNNTs is assigned to be II with a sharp peak composed of a vibrational fine structure having a π* resonance characteristic. This shows that there is a superimposition of the π* features for GN and molecular nitrogen states at II. In addition, the electron transition feature from the 1 s core to the unoccupied σ* state is denoted III. We find that the π* and σ* related peak intensity is decreased after attaching the NPs compared to NEXAFS spectra of the pristine CNNTs. The decrease in the relative peak intensity of I and III implies that the nitrogen-mediated unoccupied states from GN and PN bonds with neighboring carbon atoms are occupied after anchoring of NPs on those N sites. This indicates that both PN and GN on CNNTs contribute to the anchoring of NPs.

Fig. 4a shows the tunability of magnetization curves for pristine CNNTs and size tunable magnetite NPs–CNNT hybrids at 300 K. We determined the magnetic properties of NPs–CNNT hybrids using a vibrating sample magnetometer (VSM) and found that the pristine CNNT has non-magnetic property. Meanwhile, it is determined that magnetite NPs attached on the outer surface monolayer of a CNNT exhibit the super-paramagnetism with no coercivity or remanence. The magnetization of 7.9 nm NPs–CNNT hybrids (H-3) is 15.95 emu g^{-1} at 17 kOe. When the microwave heating time is decreased, the sizes of NPs are reduced to 4.9 nm (H-2) and 2.3 nm (H-1), respectively. These results give the corresponding magnetization values of 3.95 and 2.58 emu g^{-1} at 17 kOe, thus proving that the larger size of pure NPs would lead to higher magnetization. The response of magnetic NPs–CNNT hybrids having the water soluble property to the external magnetic field is also visualized in Fig. 4b, which implies high recovery features of the hybrid catalyst. After sonication, the NPs–CNNT hybrid

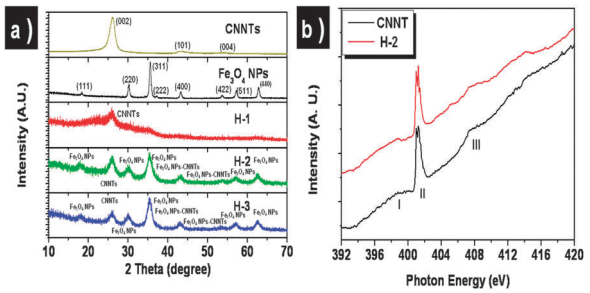

Fig. 3 (a) XRD patterns of CNNTs, pure Fe_3O_4 NPs, and NPs–CNNT hybrids fabricated in different heating times. (b) NEXAFS spectra of CNNTs and NPs–CNNT hybrids.

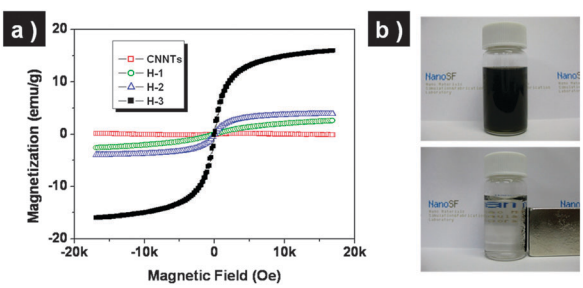

Fig. 4 (a) VSM analyses of CNNTs and NPs–CNNT hybrids with different sizes of NPs. (b) Photograph of NPs–CNNTs in water (up) and their response to the external magnetic field (down).

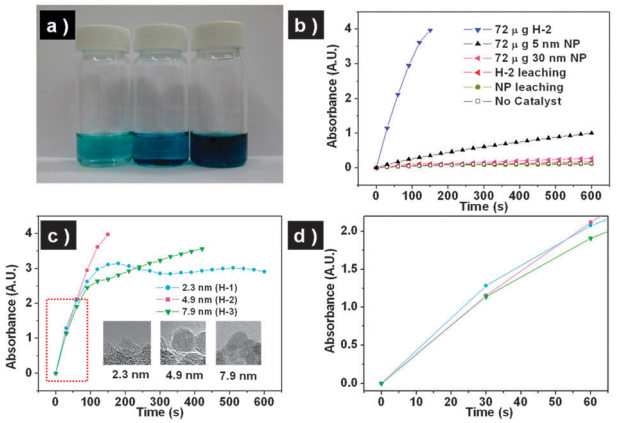

Fig. 5 (a) Photograph of the color changes attributed to the peroxidase mimetic activity tests under no catalyst (left) and in the presence of pristine magnetite NPs (middle) and magnetite NPs–CNNTs (right), (b) their activities under different conditions including the leaching solution, (c) NP size dependence for the peroxidase mimetic activities (inset: HRTEM images of NPs), and (d) their early reaction stages; shown inside the dotted rectangular area of (c).

was found to be well dispersed in water without agglomeration. The FT-IR analysis (Fig. S3, ESI†) shows that hydrophilic radicals are formed on the surfaces of NPs attached on the CNNTs.

Also, we have analyzed the peroxidase-mimetic activity of Fe_3O_4 NPs at room temperature through the measurement of the oxidation extent for a peroxidase substrate TMB by H_2O_2 to the oxidized product, where it changes to blue color through the absorbance at 652 nm as demonstrated in Fig. 5a. Fig. 5b shows that the activity for the 7.9 nm Fe_3O_4 NPs–CNNT hybrid is about 12 times higher than even that for the smaller sized pure 5 nm Fe_3O_4 NP after 90 s. This might be attributed to the high surface-to-volume ratio because the NPs–CNNT hybrid shows a relatively high surface area, while the pure Fe_3O_4 NPs show severe agglomeration (Fig. S4, ESI†). We have also studied the effect of leaching of iron ions into the buffer solution from the Fe_3O_4 NP–CNNT hybrid. To investigate the leaching effect, we incubated NPs–CNNT hybrids in the standard buffer solution with pH 3.5 for 10 min and then the hybrids were moved away from the solution with a magnet. Interestingly, the leaching solution showed a negligible activity similar to that with no catalyst. Also, no significant morphology change was observed after the leaching test (Fig. S5, ESI†). This implies that the high peroxidase mimetic activity is purely attributed to the Fe_3O_4 NPs–CNNT catalysts. Moreover, the dependence of peroxidase-mimetic activities on the size of the nanoparticle catalyst has been investigated with different NP sizes ranging from 2.3 nm through 4.9 nm to 7.9 nm, which are obtained from corresponding H-1, H-2, and H-4 conditions, respectively. On the other hand, the resulting activity, absorbance measured after 10 min, was proven to be independent of the size of NPs as depicted in Fig. 5c. H-2 (middle sized NP) showed the highest activity while H-1 showed the lowest (smallest sized NP). However, H-1 shows the higher activity than that of H-2 and H-4 from the early stage of the reaction graph (see Fig. 5d). This implies that the non-crystallized surface of a small NP might be easily poisoned, resulting in the saturated activity instantly.

We have reported a facile route to fabricate the size tunable superparamagnetic nanoparticles of uniform average size without agglomeration observed on pure nanoparticles. The N K-edge NEXAFS analysis demonstrates N-mediated anchoring. In addition, our size controlled NPs on CNNTs having the water soluble property are proven to show the superparamagnetic property ranging from 2.58 to 15.95 emu g^{-1}. In addition, the peroxidase mimetic catalytic activity of NPs–CNNTs to transform a peroxidase substrate 3,3,5,5-tetramethylbenzidine by H_2O_2 to its oxidized state has been demonstrated to be significantly higher compared to those for pure magnetite NPs. Consequently, these imply that our new approach to fabricate the size-tunable superparamagnetic NPs on carbon nitride nanotubes could provide a great route to the environmental technologies.

This work was supported by the Korea Center for Artificial Photosynthesis (NRF-2011-C1AAA001-2011-0030280) and the Hydrogen Energy R&D Center. Also, it was supported by the National Research Foundation grants (NRF-2010-0007692, NRF-2009-0094039, NRF-2011-0028737, NRF-2011-0020400, NRF-2011-0030310), and by the WCU program (R-31-2008-000-10055-0). The authors also acknowledge the use of SQUID in Korea Basic Science Institute and the experiments at PLS supported by the MEST and POSTECH.

Notes and references

1 A. P. Alivisatos, *Science*, 1996, **271**, 933.
2 Y. Sun and Y. Xia, *Science*, 2002, **298**, 2176.
3 S. I. Lim, I. Ojea-Jimnéz, M. Varon, E. Casals, J. Arbiol and V. Puntes, *Nano Lett.*, 2010, **10**, 964.
4 H. Dai, W. Wong and C. M. Lieber, *Science*, 1996, **272**, 523.
5 M. S. Dresselhaus, G. Dresselhaus and P. Avouris, *Carbon Nanotubes*, Springer, Berlin, 2001.
6 S. J. Kang, C. Kocabas, T. Ozel, M. Shim, N. Pimparkar, M. A. Alam, S. V. Rotkin and J. A. Rogers, *Nat. Nanotechnol.*, 2007, **2**, 230.
7 J. W. Lee, H. S. Kim, J. Y. Lee and J. K. Kang, *Appl. Phys. Lett.*, 2006, **88**, 143126.
8 Z. Liu, J. Wang, D. Xie and G. Chen, *Small*, 2008, **4**, 462.
9 L. Fu, Z. Liu, Y. Liu, B. Han, P. Hu, L. Cao and D. Zhu, *Adv. Mater.*, 2005, **17**, 217.
10 Y. Lee, H. J. Song, H. S. Shin, H. J. Shin and H. C. Choi, *Small*, 2005, **1**, 975.
11 V. Georgakilas, D. Gournis, V. Tzitzios, L. Pasquato, D. M. Guldi and M. Prato, *J. Mater. Chem.*, 2007, **17**, 2679.
12 J. W. Lee, R. Viswan, Y. J. Choi, Y. Lee, S. Y. Kim, J. Cho, Y. Jo and J. K. Kang, *Adv. Funct. Mater.*, 2009, **19**, 2213.
13 T. Pradeep and Anshup, *Thin Solid Films*, 2009, **517**, 6441.
14 D. Nelson and E. Elisa, *Appl. Catal., B*, 2000, **28**, 83.
15 L. Gao, J. Zhuang, L. Nie, J. Zhang, Y. Zhang, N. Gu, T. Wang, J. Feng, D. Yang, S. Perrett and X. Yan, *Nat. Nanotechnol.*, 2007, **2**, 577.
16 H. Wei and E. Wang, *Anal. Chem.*, 2008, **80**, 2250.
17 Y. Jung, Y. Huh, J. Choi, J. Lee, H. Song, S. Kim, S. Yoon, K. Kim, J. Shin, J. Suh and J. Cheon, *J. Am. Chem. Soc.*, 2005, **127**, 5732.
18 T. Hyeon, *Chem. Commun.*, 2003, 927.
19 A. K. Gupta and M. Gupta, *Biomaterials*, 2005, **26**, 3995.
20 S. C. Ray, C. W. Pao, H. M. Tsai, J. W. Chiou, W. F. Pong, C. W. Chen, M. H. Tsai, P. Papakonstantinou, L. C. Chen and K. H. Chen, *Appl. Phys. Lett.*, 2007, **91**, 202102.

